

Activating nano-bulk interplays for sustainable ammonia electrosynthesis

November 2022

Meng Li, Bin Hua, Dong Ding, Wei Wu, Lucun Wang, Robert A. Walker, Yong Ding, Martha Welander





DISCLAIMER

This information was prepared as an account of work sponsored by an agency of the U.S. Government. Neither the U.S. Government nor any agency thereof, nor any of their employees, makes any warranty, expressed or implied, or assumes any legal liability or responsibility for the accuracy, completeness, or usefulness, of any information, apparatus, product, or process disclosed, or represents that its use would not infringe privately owned rights. References herein to any specific commercial product, process, or service by trade name, trade mark, manufacturer, or otherwise, does not necessarily constitute or imply its endorsement, recommendation, or favoring by the U.S. Government or any agency thereof. The views and opinions of authors expressed herein do not necessarily state or reflect those of the U.S. Government or any agency thereof.

Activating nano-bulk interplays for sustainable ammonia electrosynthesis

Meng Li, Bin Hua, Dong Ding, Wei Wu, Lucun Wang, Robert A. Walker, Yong Ding, Martha Welander

November 2022

Idaho National Laboratory Idaho Falls, Idaho 83415

http://www.inl.gov

Prepared for the U.S. Department of Energy Under DOE Idaho Operations Office Contract DE-AC07-05ID14517

Activating nano-bulk interplays for sustainable ammonia electrosynthesis

Meng Li ^{1, 4}, Bin Hua ^{1, 4}, Wei Wu ¹, Lu-Cun Wang ¹, Yong Ding ², Märtha Welander ³, Robert A. Walker ³, Dong Ding ^{1, *}

Abstract

Small changes in a catalyst's composition, modification, and/or integration into a reactor can have significant yet often poorly understood effects on (electro)catalysis. Here we demonstrate the careful tailoring of Ru/La_{0.25}Ce_{0.75}O_{2-x} catalysts through the post-synthesized hydrothermal treatment together with control over the Ru loadings to create hydroxyl groups and electronic restructuring for ammonia electrosynthesis. When integrated into a protonic ceramic electrolyzer, the *in situ* formed Ce³⁺–OH/Ru sites facilitate both the N≡N decoupling and N–H formation at 400 °C and 1 bar of N₂, boosting the ammonia production rate (2.92 mol h⁻¹ m⁻²) up to 100-fold higher than the current state-of-the-art electrolyzers. Moreover, such catalysts and electrolyzer design concepts can be readily tuned to more complex applications such as coproducing ammonia and other chemicals with hydrocarbons as direct hydrogen sources. The creation of coordinated saturated support–OH/metal sites in the advanced electrolyzer offers an attractive approach for future clean-energy and green-chemical industries.

Keywords

Coordination saturation; Electronic restructuring; Ammonia synthesis; Carbon-based fuel conversion; Protonic ceramic electrolyzer

¹ Energy and Environmental Science and Technology, Idaho National Laboratory, Idaho Falls, ID 83415, United States.

² School of Materials Science and Engineering, Georgia Institute of Technology, Atlanta, GA 30332, United States.

³ Department of Chemistry and Biochemistry, Montana State University, Bozeman, MT 59717, United States.

⁴These authors contributed equally.

^{*} e-mail: dong.ding@inl.gov

Introduction

Ammonia is an essential precursor to a host of critical products including fertilizers and industrial feedstocks [1]. Ammonia is also being considered a promising, carbon-free energy carrier [2]. Biological nitrogen fixation in nature utilizes nitrogenase enzymes to catalyze the conversion of dinitrogen to bioavailable ammonia at ambient conditions [3, 4]. By contrast, traditional ammonia production (i.e., Haber-Bosch thermocatalytic process) is extremely energy-intensive and consumes 1-3% of the world's total annual energy supply [5, 6]. In fact, the ammonia industry produces more CO₂ than any other chemical production process. As the Haber-Bosch thermocatalytic process is already mature and unlikely to be adapted to become more environmentally friendly, the ammonia industry is considering new, transformative approaches to create ammonia using more environmentally benign means [7-10]. In principle, renewable electrosynthesis stands out as a promising solution to this challenge, but in conventional aqueous media, a large overpotential is required to achieve effective reaction rates, and the NH₃ selectivity is often low with hydrogen evolution being the primary competing reaction [11-18]. Ceramic electrolyzers promise intrinsic advantages over aqueous electrolyzers, because the thermocatalysis and electrocatalysis can be coupled to promote the reaction kinetics, and the gaseous N₂ molecules can directly diffuse to active sites without being confined by the low solubility and slow transport in liquids [19-24].

The discovery of proton-conducting ceramics (e.g., BaZr_{0.1}Ce_{0.7}Y_{0.1}Yb_{0.1}O_{3-x} (BZCYYb) and BaZr_{0.4}Ce_{0.4}Y_{0.1}Yb_{0.1}O_{3-x} (BZ₄CYYb)) and their integration into the electrocatalysis research have generated interest and promoted widespread research activity [25-31]. The electro-deprotonation and electro-protonation processes can be decoupled in proton-conducting electrolyzers (PCEs). Moreover, PCE operating temperatures (350~450 °C) are suitable for many hydrogenation and dehydrogenation reactions [32]. Leveraging these advantages so that PCEs can be used for highperformance ammonia production will require highly active and selective electrocatalysts for N₂to-NH₃ conversion. Thus far, most PCE electrocatalysts have been inspired by cathode materials used for solid oxide fuel cells (SOFCs) [33]. These materials – while functional – are not optimized for PCE specific applications such as ammonia production. In an effort to create nextgeneration electrocatalysts designed specifically for use in PCE devices, researchers have drawn on lessons learned from homogenous catalysis that show how catalysts having multiple metal centers can create more active sites N₂ dissociation and oxidation than those with single centers [34, 35]. Similarly, heterogenous thermocatalysis studies suggest that N≡N triple bond activation by several transition metal atoms is more efficient than single-site activation [36, 37]. In addition to the metal sites, the chemical environments of the topmost atomic layers (e.g., surface adsorbents) in these transition metal compounds play a crucial role in both the activity and the selectivity [38-40].

In this report, we show how careful tailoring of Ru/La_{0.25}Ce_{0.75}O_{1.875} (Ru/LDC) catalyst through the post-synthesized hydrothermal treatment together with control over the Ru loadings (0.5, 1, 2.5 and 5 wt.%) significantly enhances ammonia electrosynthesis in PCEs operating at 400 °C and 1 bar of N₂. This work chose Ru to provide active sites since it is placed at the top of the theoretical volcano plot for N₂ reduction reaction [41-44]. Our findings are supported by highlevel computational and experimental studies that highlight the creation of a coordinated saturated support-OH site along with an adjacent metal site through two consecutive processes—in situ metal (Ru) precipitation from the host lattice (Ru_{2x}La_{0.25-x}Ce_{0.75-x}O_{1.875+(x/2)}, RLCO) and steam dissociation on the oxygen vacancies of support (LDC). Accordingly, we report 1 wt.% Ru/LDC catalysts with active surface OH species (denoted as LDCRu-W) that enhance ammonia production rates by up to 100-fold higher than those of the previous N₂ electrolyzers. Moreover, we show that this N₂ electrolyzer with a proton conductor can be readily tuned to suit more complex applications with light alkane or biogas as direct hydrogen sources for the coproduction of ammonia and light alkenes and/or syngas. This study illustrates that electrocatalyst efficacy depends sensitively on not only the catalyst but also the chemistry that occurs at the catalyst-support boundary. Furthermore, these studies and the newly developed materials create a well-defined roadmap for future catalyst development and integration into emerging, environmentally-responsible technologies.

Results and Discussion

We performed extensive calculations to clarify how single supported Ru atoms (SAs, Ru1), Ru nanoclusters (NCs, Ru5) and Ru nanoparticles (NPs, Ru14) are affected by interactions with an LDC support. Of particular importance is identifying how surface OH species change the selectivity and activity of the Ru/LDC heterostructure for ammonia synthesis. Previous theoretical and experimental work has verified that atom-scale metals (NCs and SAs) can be stabilized through high adsorption energies thanks to the upshift of the metal *d* state energies on reducible oxides [45]. Given these findings, we expected to observe similar behavior for Ru SA, NC, and NP on LDC substrate where the cerium can exist as either Ce⁴⁺ or Ce³⁺. The LDC (110) terminated surface was adopted for the computational modeling studies because it is stable and experimentally available. Adsorbed OH species were considered because they are thought to be critical intermediates in many surface-driven, electrocatalytic reactions [46]. These computational studies uncovered how the evolution of both the interfacial geometrical configuration and interfacial charge transfer of the Ru/LDC heterostructure change with Ru size (SA/NC/NP) and the addition of OH groups.

We first detailed the evolution of Ru 4d orbitals through the projected density of states (PDOS) calculations (Fig. 1a). Note that RuX (X=1, 5, 14) represents the model without OH groups and H₂O RuX represents the model with OH groups. With the decrease of the Ru size from NPs

(H₂O Ru14) to NCs (H₂O Ru5), the average coordination numbers of each Ru atom decrease accompanied by increased chemical potential, making the occupied bands more discrete. Consequently, the average energies of the d states in the Ru d band centers increase. Interatomic distances reduce from their bulk values (H₂O Ru14) to stabilize the geometrical structure in the smaller one (H₂O Ru₅). Therefore, the overlap between the d orbitals on adjacent metal atoms increases, while the position of the Ru d band center is brought down from -2.01 eV (H₂O Ru14) to -2.34 eV (H₂O Ru₅). Further reduction in the Ru size from NC (H₂O Ru₅) to SA (H₂O Ru₁) or removal of the OH species (Ru5) results in a shift of the Ru d band centers to higher (or less stable) energies: the Ru d band center values are -1.63 eV and -2.19 eV for H₂O_Ru1 and Ru5, respectively. Similar trends occur in the difference maps of electron density that represent electron accumulation and depletion on the Ru/LDC heterostructure (Fig. 1b and Supplementary Fig. 1). The total electrons transferring from Ru species to LDC is more pronounced in H₂O Ru5 in comparison with those of H₂O Ru1 and H₂O Ru14. The total electrons transfer increases remarkably in H₂O Ru5 (2.4839). The orbital and electron distributions in the H₂O Ru5 model are extensively delocalized compared with H₂O-free Ru5 model, implying strong synergy between adsorbed OH and the LDC support that contributes to the system's overall reactivity. These findings provide guidance for changing catalyst/support band structure to optimize N₂ splitting and protonation for ammonia synthesis.

The thermodynamics of elementary reactions is fundamental to the understanding of catalytic reactions at surfaces. Therefore, we investigated the $N_2 + 3H_2 = 2NH_3$ reactions over the catalysts to examine the effects of OH species and Ru size on reaction pathways. Both an "associative mechanism" and a "dissociative mechanism" were investigated using density functional theory (DFT) calculations (Supplementary Fig. 2) [47]. The optimized Gibbs free energy diagrams at 400 °C are summarized in Fig. 1c (the associative mechanism) and 1d (the dissociative mechanism). More details about the elementary models, Gibbs free energy calculation method, as well as zero-point energy and entropy corrections, are presented in Supplementary method, Supplementary Tables 1-2 and Supplementary Figures 3-8. The calculation profiles show that the surface OH groups and an optimized Ru size can lower the energy barrier for the reactions that lead to ammonia synthesis. Compared with the H₂O_Ru1 and H₂O_Ru14, the suitable mixed ionic and metallic feature of H₂O_Ru5 significantly reduces the energy barriers for N₂ adsorption and splitting in both the "associative mechanism" (* \rightarrow *N₂ \rightarrow *NNH) and the "dissociative mechanism" (* \rightarrow *N₂ \rightarrow *N+*NH). Furthermore, the addition of OH promotes the protonation steps during the ammonia synthesis processes, i.e., *NNH--*NHNH in the "associative mechanism" and *N→*NH in the "dissociative mechanism". These results strongly support the idea that the addition of surface hydroxy as well as optimized mixed ionic and metallic features of Ru are essential to the promoted catalytic activity for NH₃ synthesis.

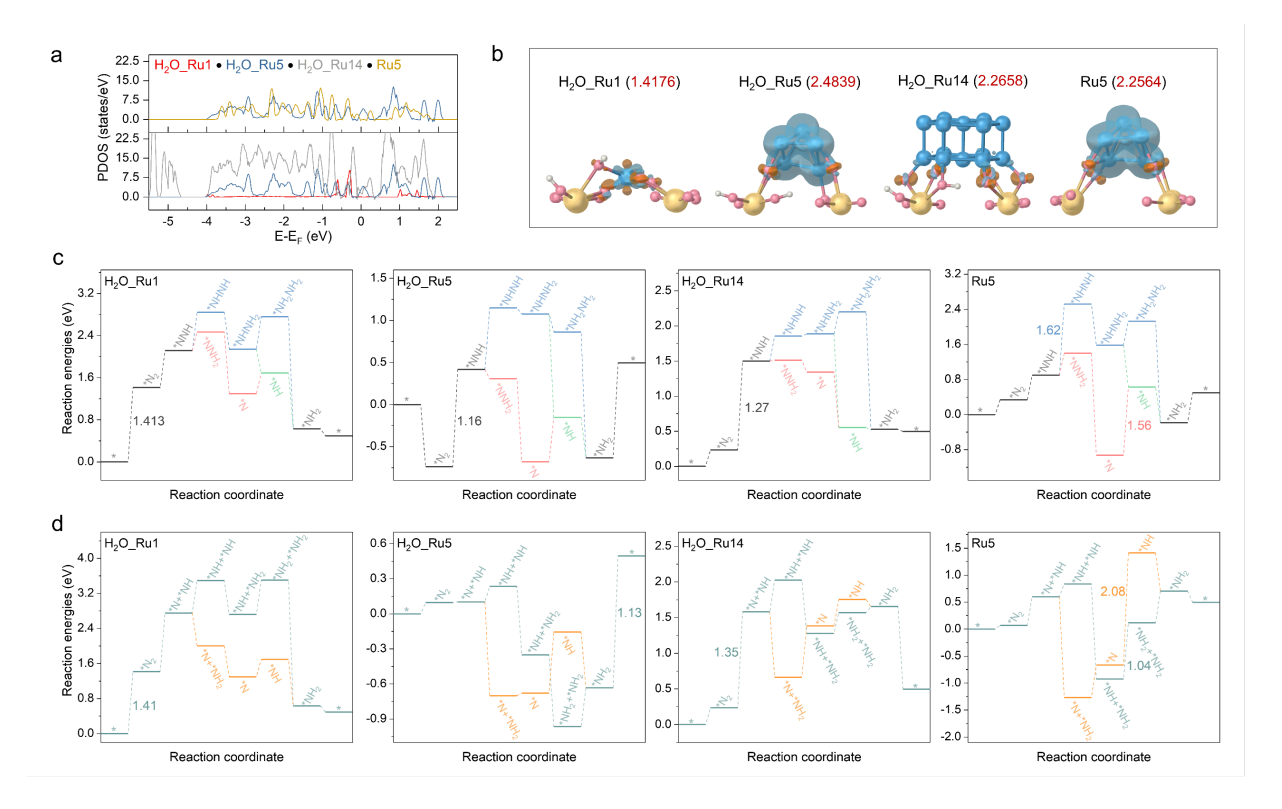


Figure 1. Theoretical calculations for catalyst design. a, Projected density of states of Ru 4*d* orbitals in H₂O_Ru1, H₂O_Ru5, H₂O_Ru14, and Ru5 models; b, The difference maps of the electron and the total electron loss in the H₂O_Ru1, H₂O_Ru5, H₂O_Ru14, and Ru5 models. Orange and blue isosurfaces exhibit the accumulation and depletion of electron density at the isovalue of 0.03 e Bohr⁻³; c, Gibbs free energies of optimized elementary reactions over H₂O_Ru1, H₂O_Ru5, H₂O_Ru14, and Ru5 models based on the associative mechanism; d, Gibbs free energies of optimized elementary reactions over H₂O_Ru1, H₂O_Ru5, H₂O_Ru14, and Ru5 models based on the dissociative mechanism.

Given predictions from the DFT studies, we sought to design and test these catalysts experimentally. We developed a novel hydrothermal exsolution method to synthesize the Ru/LDC model catalysts. Specific details about catalyst synthesis are included in Supplementary method. The exsolution synthesis method relies on the homogeneous incorporation of Ru cations into the LDC host lattice. The complexing agents were added to promote the hydrolysis reaction, ensuring the high dispersion of the metal cations during the gel preparation (Fig. 2a). Gel precursors were calcined under the oxidizing condition to produce a series of RLCO tri-metal oxide solid solutions. A facile hydrothermal exsolution process was carried out in wet H₂ at 400 °C (wet represents 3% H₂O). With this treatment, we anticipated that Ru cations were exsolved from the fluorite lattice to form well-distributed Ru/LDC heterostructures with multiple *OH species anchoring on the surface oxygen vacancies. The X-ray diffraction pattern (XRD) analysis has confirmed the redox process of the Ru cations—The Ru cations substitute Ce or La in the

fluorite structure in the air calcination step (Supplementary Fig. 9a and 9b) and exsolve from the RLCO tri-metal oxide in the hydrothermal reduction step (Supplementary Fig. 9c and 9d). Fig. 2b and Supplementary Fig. 10 and 11 display representative high-angle annular dark-field–scanning transmission electron microscopy (HAADF–STEM) images and STEM–Energy-dispersive X-ray spectroscopy (EDX) results of the as-synthesized Ru/LDC catalysts with different Ru loadings (0.5, 1, 2.5 and 5 wt.%). High resolution STEM images show the presence of exsolved Ru species with dimensions depending on the Ru loadings (Fig. 2b). As the Ru content increases, the coordination numbers of Ru atoms increase as does particle size. Ru appears in atomic size in Ru/LDC with 0.5 wt.% loading. Ru particle sizes fall in the range of 0.2-0.9, 1-2, and 2.5-3.5 nm for Ru loadings of 1, 2.5, and 5 wt.%, respectively. Their corresponding average particle sizes are 0.7, 1.7, and 3.1 nm. The chemical composition analysis verifies the creation of well-distributed, size-varied Ru/LDC heterostructures (Supplementary Fig. 10). By contrast, there are no Ru NPs/NCs present in the pristine RLCO solid solutions (Supplementary Fig. 11), confirming our expectation, namely that Ru atoms were first incorporated into the lattice during calcination in the air and then exsolved from the solid solution on hydrothermal reduction.

We investigated these model catalysts to validate the Ru-size-dependent activity and selectivity predicted by the DFT calculations. The catalytic performance for NH₃ synthesis was evaluated at 400 °C and 1 bar in the presence of H₂ using an H₂/N₂ ratio of 3/1. Initially, the effect of the Ru size was studied using the Ru/LDC catalysts (Ru=0, 0.5, 1, 2.5, and 5 wt.%). To investigate the effect of Ru size, all the catalysts were pretreated in dry H₂/Ar at 400 °C to remove the surface OH species. The NH₃ production rates (PRs) are reported in Fig. 2c. Control experiments carried out with the LDC support showed the substrate to be inactive for NH₃ synthesis. Under dry conditions, the 1 wt.% Ru/LDC (LDCRu-D, D represents dry) is the most effective catalyst for ammonia synthesis, delivering a PR of 3.12 mmol h⁻¹ g⁻¹. Such a catalyst is superior to the impregnated LDC/1% Ru (1.50 mmol h⁻¹ g⁻¹) and impregnated LDC/5% Ru (2.41 mmol h⁻¹ g⁻¹)—already identified as a state-of-the-art NH₃ synthesis catalyst [48]. The catalysts with higher Ru loadings (2.5 and 5 wt.%) do not deliver higher NH₃ PRs, indicating 1 wt.% Ru is the optimal loading on LDC support. Finally, the 1 wt.% Ru/LDC pretreated in wet H₂/Ar (LDCRu-W, W represents wet with 3% H₂O) was tested in wet H₂/N₂ to reserve their OH species. The addition of OH species enhances NH₃ PR to 3.62 mmol h⁻¹ g⁻¹. In line with expectations from the DFT results, both the surface hydroxyl and the Ru size appear to be essential for optimal NH₃ production.

Seeking to clarify further how size, structure, and electronic states of the Ru species change the catalytic performance experimentally, we performed a series of spectroscopic characterizations. Fig. 2d and supplementary Fig. 13 show the X-ray photoelectron spectroscopy (XPS) data from the Ru/LDC catalysts [49]. The Ru 3d peak exhibits a negative shift with the increase of the Ru

loadings. The reducible LDC supports can act as the electron acceptor, capturing the electrons from Ru species. Such a charge transfer effect is enhanced by decreasing the Ru size (*c.f.*, TEM images in Fig. 2b and XPS in Fig. 2d). CO-Diffuse Reflectance Infrared Fourier Transform Spectroscopy (CO-DRIFTS) was performed to analyze the bonding states of the Ru surface species (Fig. 2e). The 0.5 wt.% Ru/LDC catalyst shows only linear and geminal CO peaks (above 2000 cm⁻¹), without any bridge or three-fold hollow peaks from the Ru NPs or NCs. This result verifies that 0.5 wt.% Ru/LDC catalyst seems to have a single atom structure [50, 51]. In the case of 1 wt.% Ru/LDC catalyst, there is a bridge CO peak at 1990 cm⁻¹, while for the 2.5 and 5 wt.% Ru/LDC catalysts, DRIFTS spectra CO adsorption peaks below 2000 cm⁻¹ indicating CO binding to multiple bridging or three-fold hollow sites [52, 53]. The CO-DRIFTS results reveal that the degree of Ru agglomeration is correlated positively with the Ru loading. The 1 wt.% Ru/LDC leads to a suitable mixed ionic and metallic character that we ascribe to this system's high NH₃ PR activity.

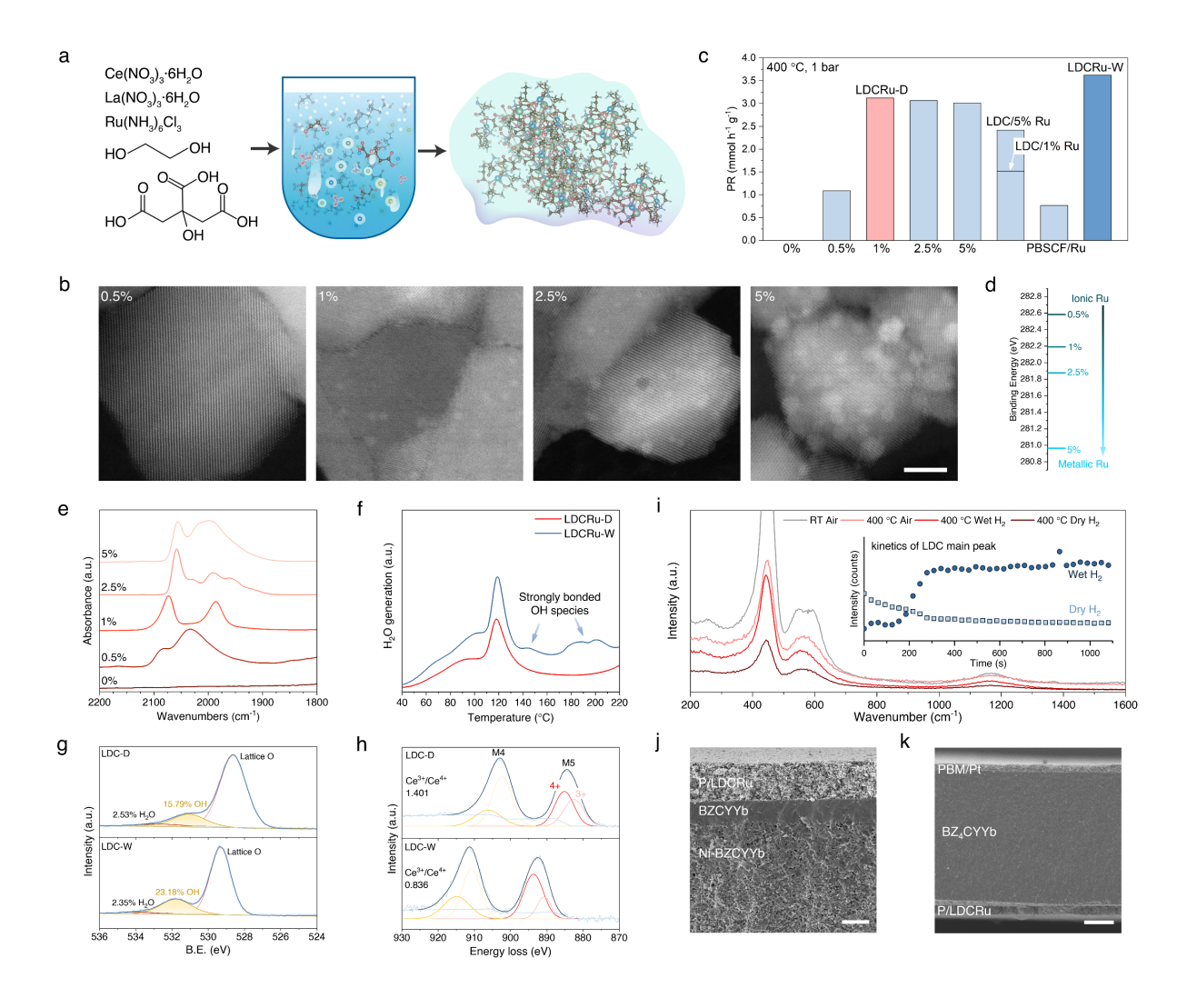


Figure 2. Materials synthesis and physical characterization. a, Schematic illustration of the gel preparation process for the Ru/LDC catalysts with various Ru loadings; b, STEM-HAADF images of the as-synthesized Ru/LDC catalysts with different Ru loadings (0.5, 1, 2.5 and 5 wt.%). The scale bars represent 5 nm; c, The catalytic performance of various catalysts for NH₃ synthesis at 400 °C and 1 bar in the presence of H₂ using an H₂/N₂ ratio of 3/1; d, The position of the XPS Ru 3*d* peak with different Ru loadings (0.5, 1, 2.5 and 5 wt.%); e, CO-DRIFTS spectrum of the as-synthesized Ru/LDC catalysts with different Ru loadings (0.5, 1, 2.5 and 5 wt.%), and the CO-DRIFTS spectrum of LDC is also illustrated for a companion; f, H₂-TPR profiles of LDCRu-D and LDCRu-W catalysts in dry H₂/Ar; g, XPS O 1*s* peaks for LDC-D and LDC-W; h, EELS Ce $M_{4,5}$ edges for LDC-D and LDC-W; i, *operando* Raman tests over the pure LDC powder by changing the humidity of the flowing gas. The scale bar represents 20 μm; j and k, SEM cross-section of two types of PCEs, the scale bar represents 50 μm.

We then sought to establish the correlation of OH species with the reaction activity. Fig. 2f exhibits the H_2 -temperature programmed reduction (H_2 -TPR) profiles of LDCRu-D and LDCRu-W catalysts in dry H_2 /Ar. For both samples, the broad peaks below 100 °C can be assigned to the weakly bonded surface oxygen species, and the sharp peaks at around 120 °C are from the reduction of Ru oxides [54]. Over LDCRu-W, extra peaks marked by the blue arrows are most likely caused by the desorption of the strongly bonded OH species on the LDC support [55, 56]. Nitrogen protonation can be promoted by the OH species, but on LDCRu-D, surface hydroxy species are absent and cannot play a role. Over LDCRu-W, time-resolved DRIFTS has shown that the intensity of the N-H stretch increases along with the increase of -OH stretch in the wet H_2/N_2 flow at 400 °C, while over LDCRu-D, the intensity of the N-H stretch decreases substantially along with the decrease of -OH stretch in the dry H_2/N_2 flow at 400 °C (supplementary Fig. 14). These results strongly imply that the N-H bonds are more readily created with assistance from surface OH species.

To clarify the interaction of OH species with the LDC support, we conducted a series of independent characterizations using pure LDC powders. These measurements were carried out specifically to assess how adsorbed OH affects the redox state of elements in the LDC. The pure LDC powders were treated in dry H₂/Ar and wet H₂/Ar, respectively, to prepare the LDC-D and LDC-W samples. Fig. 2g shows the O 1s XPS spectra that can be revolved into three sub-peaks, *i.e.*, adsorbed water, hydroxyl group (-OH), and lattice oxygen [57]. The fractional intensity from hydroxyl groups rises from ~16 % in LDC-D to ~23 % in LDC-W, while the amount of the adsorbed water does not change, emphasizing that wet preparation methods can increase surface hydroxyl groups by as much as 50%. The increase in hydroxyl groups is also indicated by the shift in lattice oxygen peak position which is caused by changes in oxygen vacancy concentration [58]. The interaction between OH and LDC support was also verified by the electron energy loss

near edge structure of LDC-D and LDC-W via the electron energy loss spectroscopy (EELS) analysis. Because of the existence of a significant amount of hydroxyl groups on the LDC-W surface, the valence of Ce (Ce³⁺/Ce⁴⁺=1.401) in LDC-D represents a significant negative shift in reference to that in LDC-W (Ce³⁺/Ce⁴⁺=0.836) (Fig. 2h). To directly investigate the strong interaction of OH species with the LDC support, we performed operando Raman tests over the pure LDC powder by changing the humidity of the flowing gas (Fig. 2i). After taking a Raman spectrum at room temperature in air (RT air), the LDC powder was heated up to 400 °C in air. The RT air spectrum shows a strong ceria band at 450 cm⁻¹ and then two smaller, incompletely resolved peaks at 548 and 595 cm⁻¹ that are expected for Ce³⁺ [59]. Heating up the LDC to 400 °C in air led to a three-fold loss in intensity, and only the single high frequency band at 566 cm⁻¹ remained. When the flowing gas was changed over to a dry H₂ atmosphere, a further intensity loss and a 6-10 cm⁻¹ red shift in the vibrational features are observed. This result is consistent with a Ce⁴⁺ to Ce³⁺ reduction arising from oxygen loss and a weakening of the lattice bonds. These changes were reversible, with intensity returning when the gas was switched to a wet H₂ atmosphere. Repeated cycling between dry and wet H₂ atmospheres resulted in quantitative switching between low and high intensities and peak shifts, indicating that labile OH species on the LDC support can be controlled easily by changing the humidity.

In light of discovering such an active catalyst for NH_3 synthesis, we integrated the LDCRu-W catalyst into a PCE to demonstrate its effect on electrochemical NH_3 synthesis. As displayed in Fig. 2j-2k, two types of PCEs were fabricated. The PCE-1 (Fig. 2j) consists of a Ni-BZCYYb composite anode, a PBSCF cathode (Supplementary Fig. 15), and a thin BZCYYb electrolyte. PCE-2 (Fig. 2k) is composed of a PrBaMn₂O_{5+ δ} + Pt (PBM/Pt) anode, a PBSCF cathode, and a thick BZ₄CYYb electrolyte support (BZCYYb-S, Fig. 2j). In both PCE-1 and PCE-2, the LDCRu-W catalyst was impregnated into the PBSCF cathode to prepare the P/LDCRu-W electrodes for N_2 -to- NH_3 conversion. As benchmarks, Ru + PBSCF (P/Ru) and LDCRu-D + PBSCF (P/LDCRu-D) cathodes were prepared *via* the impregnation method.

We compared the selectivity and activity of three cathodes for NH₃ production to prove that this catalyst design concept is valid in the electrocatalysis mode. To simplify the chemistry responsible for ammonia production, H₂ rather than more complex hydrogen sources was used. Because the Ni-BZCYYb anode has long been considered as a very good electrocatalyst for H₂ activation and oxidation into protons, cell configuration of PCE-1 was used to compare the P/LDCRu-W, P/LDCRu-D and P/Ru cathodes. During the electrocatalysis, Ni-BZCYYb captures the protons from H₂ (3H₂ – 6e⁻ = 6H⁺), while N₂ reduction reaction (N₂ – 6e⁻ + 6H⁺= 2NH₃) and competing hydrogen evolution reaction (6H⁺ + 6e⁻ = 3H₂) take place at the cathode. The selectivity and activity for NH₃ synthesis are thus dependent on the cathodes. The electrochemical measurements were carried out at 400 °C in flowing N₂ (20 ml min⁻¹) and H₂ (60

ml min⁻¹). The flowing N₂ in P/LDCRu-W cathode was humidified to create surface OH groups. The electrochemical potential measurements demonstrated that all the PCEs have similar performance for the NH₃ production and H₂ permeation (Supplementary Fig. 16), indicating each cathode's functional performance. To test whether the LDCRu-W catalysts would significantly improve the NH₃ selectivity, the short-term chronoamperometric measurements were carried out to acquire the accurate current density and NH₃ PR at certain potential bias for each PCE (Supplementary Fig. 17). The NH₃ PRs were demonstrated by a Nessler reagent colorimetric method. Figs. 3a-3d show the total current density, NH₃ partial Faradaic efficiency (FE), NH₃ partial current density and NH₃ PR over the three cathodes. Under increased working potential and current density outputs, the P/LDCRu-W cathode provides the highest NH₃ PR of 2.92 mol $h^{-1}\ m^{-2}$ and a NH $_3$ partial FE of 23.1 % at a potential bias (E $_{bias}$) of 0.6 V. Control experiments using an Ar or Ar-diluted N_2 reaction gases at 400 °C and E_{bias} of 0.6 V confirmed the reduction of N₂ in the P/LDCRu-W cathode (Supplementary Fig. 18). More importantly, the P/LDCRu-W cathode provided a stable current density for the NH₃ production and reproducible NH₃ PR and FE over a wide range of E_{bias} window (Fig. 3a-3d and Supplementary Fig. 17-19). In the case of P/Ru and P/LDCRu-D cathodes, the NH₃ partial current densities demonstrate a slow growth with the increase of total current densities when the E_{bias} is higher than 0.3 V. This result indicates high selectivity for hydrogen evolution reaction at higher Ebias. The highest NH₃ partial FEs over P/Ru and P/LDCRu-D cathodes are only 5.5 % and 14.3 %, and occur at very low current densities with E_{bias} of 0.3 V. These results demonstrate clearly that the P/LDCRu-W cathode remarkably enhances the selective N₂ reduction in electrocatalysis mode, boosting the ammonia production rate up to 100-fold higher than the state-of-the-art N₂ electrolyzers (Tables S3).

Inspired by the promising electrochemical results, we tested the robustness of the P/LDCRu-W cathode for ammonia electrosynthesis. The chronoamperometric technique was used to continuously record PCE current densities at 400 °C and 0.6 V while exposed to a flowing wet N₂ atmosphere. The in-line NH₃ PRs over the P/LDCRu-W cathode were analyzed by a Nessler reagent colorimetric method. The in-line NH₃ partial Faradaic efficiencies were calculated from these data. Fig. 3e depicts results from prolonged catalytic and electrocatalytic PCE performance operating under these conditions. The data show that output current densities stabilize in the range of 99-101 mA cm⁻² and show no attenuation during the ~560 h stability test. Most importantly, NH₃ selectivity is preserved at around 22%, suggesting that the P/LDCRu-W cathode is stable for NH₃ electrosynthesis. These findings further illustrate how careful tailoring of the post-synthesized hydrothermal treatment together with control over the metal loading enables the highly efficient and robust NH₃ production.

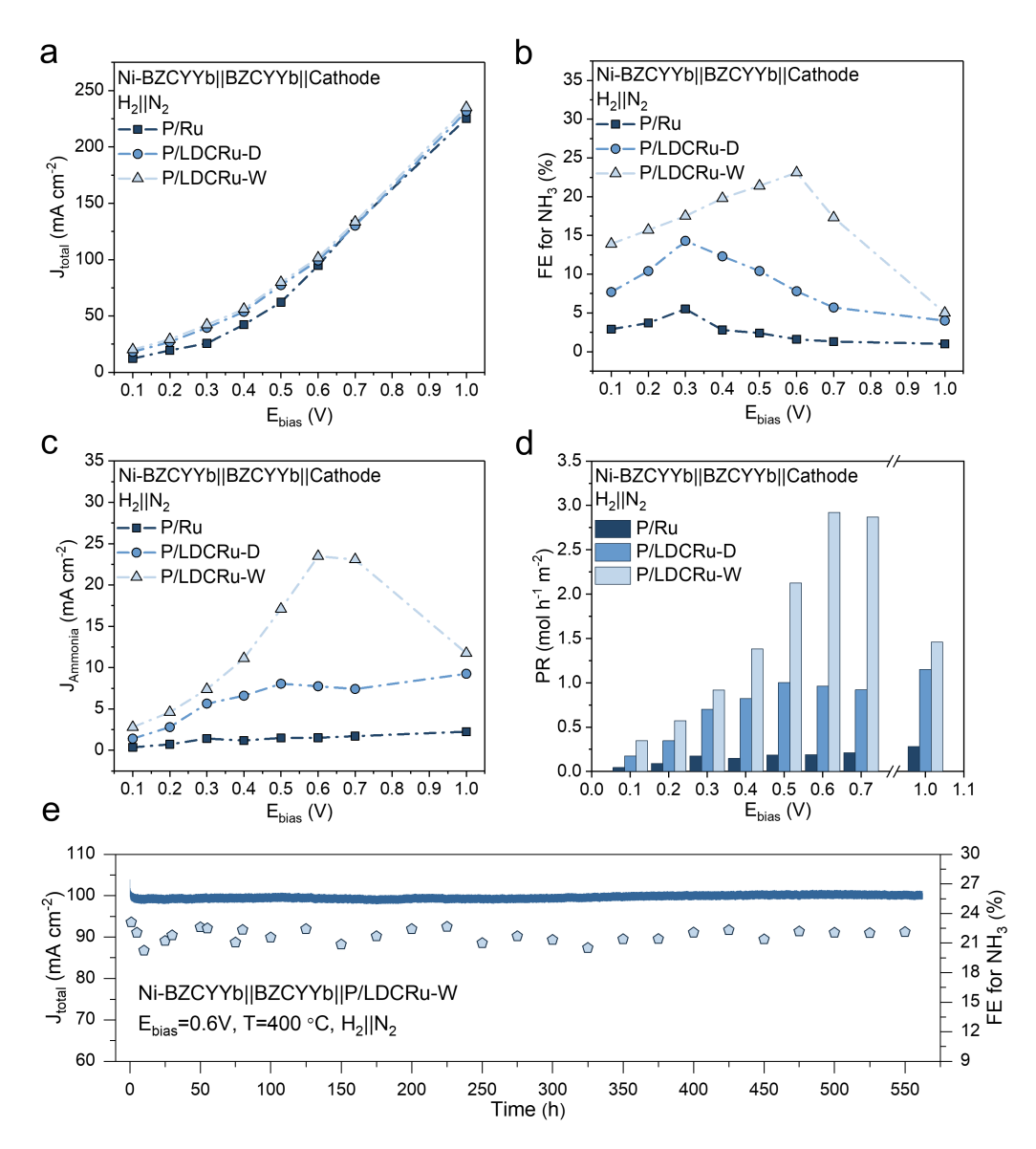


Figure 3. Comparison of various cathodes for ammonia electrosynthesis. a, polarization curves obtained from the chronoamperometric measurements at 400 °C for PCE-1 with P/LDCRu-W, P/LDCRu-D and P/Ru cathodes; b c, and d, corresponding partial Faraday efficiencies, partial current densities and production rates for ammonia over PCE-1 with P/LDCRu-W, P/LDCRu-D and P/Ru cathodes; e, long term stability test of P/LDCRu-W cathode for ammonia synthesis at 400 °C and E_{bias} of 0.6 V.

In industrial plants using the Haber-Bosch process to produce ammonia, hydrogen is generated by steam reforming of methane and water gas shift reactions, leading to significant energy consumption and CO₂ emission. PCE technology is capable of integrating these steps to enable sustainable NH₃ production. Specifically, PCEs can directly use renewable hydrogen sources (*e.g.*, CH₄-CO₂ and C₂H₆) to produce NH₃ according to the following reactions.

Anode

$$CO_2 + CH_4 - 4e^- = 2CO + 4H^+$$
 (1)

$$C_2H_6 - 2e^- = C_2H_4 + 2H^+ \tag{2}$$

Cathode

$$N_2 + 6H^+ + 6e^- = 2NH_3 \tag{3}$$

$$2H^{+} + 2e^{-} = H_{2} \tag{4}$$

These hydrogen sources are renewable and/or have abundant reserves. CH_4 - CO_2 is the main component of the biogas, while the C_2H_6 is the second largest component in natural gas. In addition to ammonia production at the cathode, PCEs can also generate CO-enriched syngas or ethylene at the anode without using intensive energy input and complex procedures. To test whether or not the Ru-LDC catalysts could also promote these ancillary processes, we first conducted thermodynamic calculations to determine if the proposed approach were possible (supplementary Fig. 20). Assuming the ambient pressure and allowing the temperature to vary from 50 to 850 °C, these studies revealed that the two processes – NH_3 production and CO-enriched syngas generation/ C_2H_6 dehydrogenation – can take place with low overpotentials. At 400 °C, the theoretical E_{bias} are only ~0.260 V and ~0.358 V with CH_4 - CO_2 and C_2H_6 feedstocks, respectively, implying that the proposed processes are thermodynamically favorable.

We fabricated a second PCE (denoted as PCE-2) with a P/LDCRu-W cathode, PBM/Pt anode, and BZCYYb-S support to test the viability of these processes with 'green' or renewable feedstocks. PCE-2 used PBM + Pt as the anode catalyst given its high activity for both methane dry reforming and C₂H₆ conversion reactions. BZ₄CYYb was used as the electrolyte to improve the chemical stability of the PCE when operating with carbon-based fuels. All electrochemical measurements were carried out at 400 °C. The cathode and the anode were exposed to flowing wet N_2 (20 ml min⁻¹) and flowing C_2H_6 (60 ml min⁻¹)/ CH_4 - CO_2 (CH_4 : CO_2 =1:1, 60 ml min⁻¹), respectively. Fig. 4a-4b and supplementary Fig 20 display the total current density, NH₃ partial current density, NH₃ partial FE, and NH₃ PR over the PCE-2 for tandem electrocatalysis of dry reforming and ammonia synthesis. Under ascending operating potential and current density outputs, the P/LDCRu-W cathode provides the highest NH₃ PR of 0.452 mol h⁻¹ m⁻² with E_{bias} = 1.5 V and the highest NH₃ partial FE of 36.5 % at E_{bias} of 0.6 V using CH₄-CO₂ as the hydrogen source. When C₂H₆ was used as the anode's hydrogen source, the highest NH₃ PR is 0.840 mol h⁻¹ m⁻² with an E_{bias} of 1.2 V, while the highest NH₃ partial FE is 35.0 % at E_{bias} of 0.6 V (Fig. 4c-4d and supplementary Fig 21). Since the PCE-2 used the thick electrolyte, the device's ohmic resistance increased significantly during the electrolysis meaning that a higher overpotential had to be applied to achieve reasonable current densities. Although the performance is not as good as that obtained in PCE-1 using H₂ as the proton source, we note that the NH₃ PR in the PCE-2 using high energy carrier hydrogen resources is still comparable to state-of-the-art N₂ electrolyzers that are based on the H₂. More importantly, such good electrocatalytic activity for NH₃ production using various hydrogen sources can be sustained in the long-term stability evaluations with varied E_{bias} and anode gas feeds (Fig. 4e, supplementary Fig. 23 and supplementary Fig. 24). These results imply that the catalyst and electrolyzer design concept can be readily tuned to address a wide range of complex catalytic and electrocatalytic applications. Chief among these is the electrochemical production of NH₃ in a sustainable, energy efficient way. This capability allows for device modularity and flexibility to adapt to the hydrogen source and the size/need of the intended application.

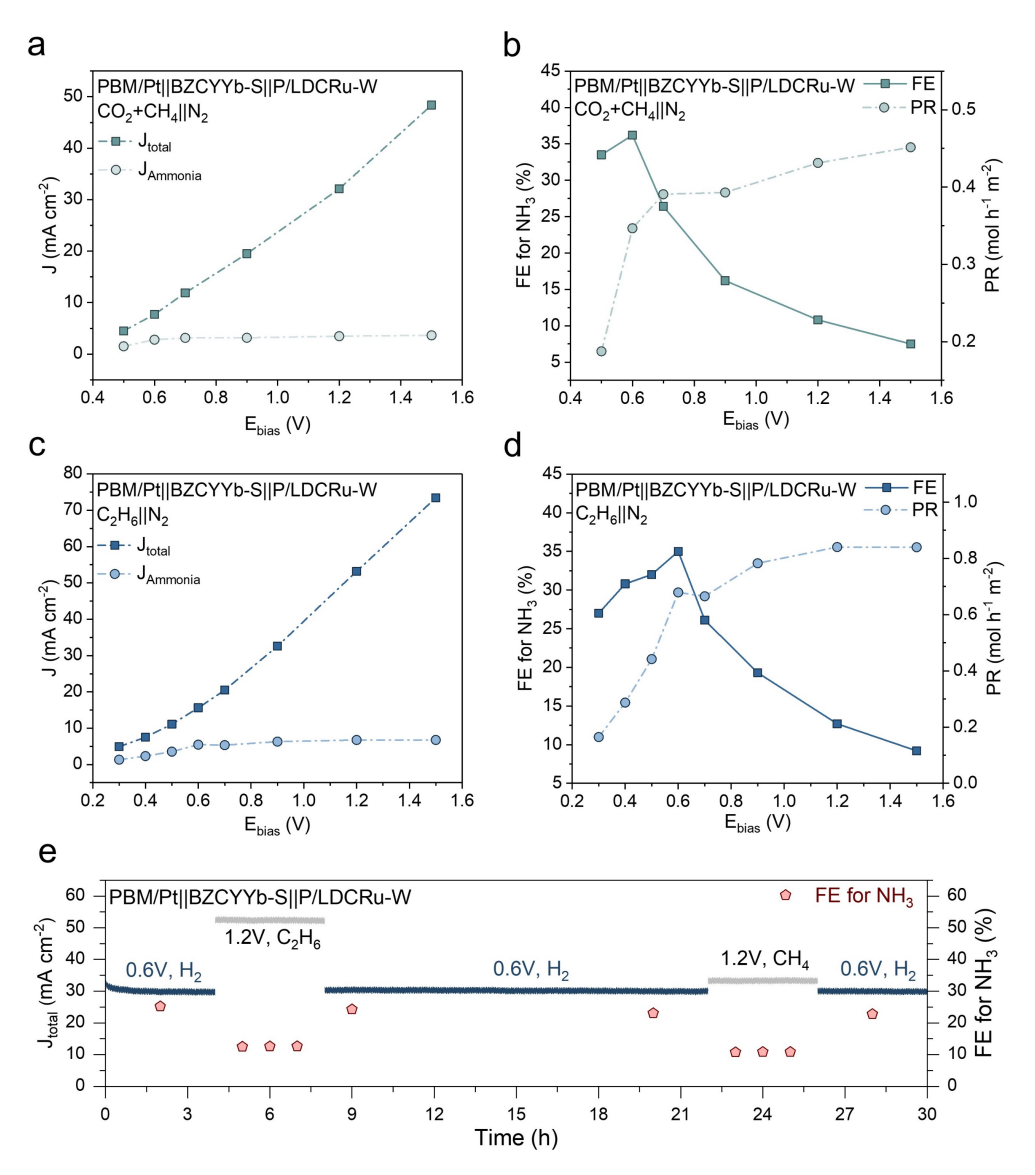


Figure 4. Demonstration of ammonia electrosynthesis from various renewable hydrogens. a and b, total current density and partial current density, and corresponding partial Faraday efficiencies and production rates of PCE-2 with P/LDCRu-W cathode for ammonia production using CO₂+CH₄ as the hydrogen source at different E_{bias} and 400 °C; c and d, total current density

and partial current density, and corresponding partial Faraday efficiencies and production rates of PCE-2 with P/LDCRu-W cathode for ammonia production using C_2H_6 as the hydrogen source at different E_{bias} and 400 °C; e, long term stability test of P/LDCRu-W cathode for ammonia synthesis at 400 °C with various hydrogen sources.

Conclusions

Work described in this report developed an efficient heterogeneous catalytic system for the electrosynthesis of NH₃. Using both theoretical and experimental results in concert, this work shows how creation of coordinated saturated support—OH/Ru NC sites along with a high performance PCE boosts ammonia production rates by up to 100-fold relative to current state-of-the-art electrolyzers. We further explored a process using renewable hydrogen containing feedstocks that combines hydrogen production and extraction, carbon-based fuel conversion, as well as ammonia production in one device and in one step, making it possible to bring the ammonia industry closer to becoming efficient and sustainable. These demonstrations of catalyst development and device integration, along with the chemical process design and integration, have paved the way for future energy-efficient industrial methods.

Acknowledgements

This work is supported by the Idaho National Laboratory Laboratory Directed Research & Development program under the Department of Energy Idaho Operations Office Contract DE-AC07-051D14517. This research made use Idaho National Laboratory computing resources which are supported by the Office of Nuclear Energy of the U.S. Department of Energy and the Nuclear Science User Facilities under Contract No. DE-AC07-05ID14517. RW and MMW gratefully acknowledge partial support from the National Science Foundation, grant number CHE-1710695.

Author contributions

M.L. and B.H. contributed equally to this work. D.D. leaded the project. B.H. and M.L. proposed the catalyst and device design concept. M.L. and B.H. did the *ab initio* calculations, developed the catalysts, integrated the electrolyzers, performed the characterizations, conducted electrochemical tests and analyzed the data. L.-C.W. helped with the DRIFTS tests. W.W. helped with the cell fabrication. Y.D. performed the TEM test. M.W. and R.A.W. performed Raman test and analyzed the results. M.L. and B.H. wrote the manuscript, and all authors contributed to the revision.

Data availability. Additional methods and results are provided in the Supplementary Information. All data supporting the findings of this study are available upon request from the corresponding author.

Competing interests

The authors declare no competing interests.

Supplementary materials

Materials and methods
Tables S1-S3
Figs. S1-S23
References (1-8)

References

- 1. J.W. Erisman, M.A. Sutton, J. Galloway, Z. Klimont, W. Winiwarter, How a century of ammonia synthesis changed the world, Nat. Geosci. 1 (2008) 636-639. https://doi.org/10.1038/ngeo325.
 - 2. A. Valera-Medina, H. Xiao, M. Owen-Jones, W.I.F. David, P.J. Bowen, Ammonia for power, Prog. Energy Combust. Sci. 69 (2018) 63-102. https://doi.org/10.1016/j.pecs.2018.07.001.
 - 3. N. Gruber, J.N. Galloway, An Earth-system perspective of the global nitrogen cycle, Nature 451 (2008) 293-296. https://doi.org/10.1038/nature06592.
 - 4. J.N. Galloway, A. R. Townsend, J. W. Erisman, M. Berkunda, Z. Cai, J. R. Freney, L. A. Martinelli, S. P. Seitzinger, M. A. Sutton, Transformation of the nitrogen cycle: recent trends, questions, and potential solutions, Science 320 (2008) 889-892. https://doi.org/10.1126/science.1136674.
 - 5. J. Rockström, *et al.* A safe operating space for humanity, Nature 461 (2009) 472-475. https://doi.org/10.1038/461472a.
 - 6. C. Smith, A. K. Hill, L. Torrente-Murciano, Current and future role of Haber–Bosch ammonia in a carbon-free energy landscape, Energy Environ. Sci. 13 (2020) 331-344. https://doi.org/10.1039/C9EE02873K.
 - 7. R. Schlögl, Catalytic synthesis of ammonia—A "Never-Ending Story"? Angew. Chem. Int. Ed. 42 (2003) 2004-2008. https://doi.org/10.1002/anie.200301553.
 - 8. E. R. Morgan, J. F. Manwell, J. G. McGowan, Sustainable ammonia production from U.S. offshore wind farms: A techno-economic review, ACS Sustain. Chem. Eng. 5 (2017) 9554-9567. https://doi.org/10.1021/acssuschemeng.7b02070.
 - 9. R. Hawtof, S. Ghosh, E. Guarr, C. Xu, R. M. Sankaran, J. N. Renner, Catalyst-free, highly selective synthesis of ammonia from nitrogen and water by a plasma electrolytic system, Sci. Adv. 5 (2019) eaat5778. https://doi.org/10.1126/sciadv.aat5778.
 - 10. P. Wang, F. Chang, W. Gao, J. Guo, G. Wu, T. He, P. Chen, Breaking scaling relations to achieve low-temperature ammonia synthesis through LiH-mediated nitrogen transfer and hydrogenation, Nat. Chem. 9 (2017) 64-70. https://doi.org/10.1038/nchem.2595.
 - 11. G. Soloveichik, Electrochemical synthesis of ammonia as a potential alternative to the Haber–Bosch process, Nat. Catal. 2 (2019) 377-380. https://doi.org/10.1038/s41929-019-0280-0.
 - 12. G.-F. Chen, Y. Yuan, H. Jiang, S.-Y. Ren, L.-X. Ding, L. Ma, T. Wu, J. Lu, H. Wang, Electrochemical reduction of nitrate to ammonia via direct eight-electron transfer

- using a copper–molecular solid catalyst, Nat. Energy 5 (2020) 605-613. https://doi.org/10.1038/s41560-020-0654-1.
- 13. F. Jiao, B. Xu, Electrochemical ammonia synthesis and ammonia fuel cells, Adv. Mater. 31 (2019) 1805173. https://doi.org/10.1002/adma.201805173.
- 14. H. Tao, *et al.* Nitrogen fixation by Ru single-atom electrocatalytic reduction, Chem 5 (2019) 204-214. https://doi.org/10.1016/j.chempr.2018.10.007.
- 15. Y. Luo, S. Liang, X. Wang, B. Lin, C. Chen, L. Jiang, Facile synthesis and high-value utilization of ammonia, Chin. J. Chem. 40 (2022) 953-964. https://doi.org/10.1002/cjoc.202100826.
- 16. W. Liao, H.-X. Liu, L. Qi, S. Liang, Y. Luo, F. Liu, X. Wang, C.-R. Chang, J. Zhang, L. Jiang, Lithium/bismuth co-functionalized phosphotungstic acid catalyst for promoting dinitrogen electroreduction with high Faradaic efficiency, Cell Rep. Phys. Sci. 2 (2021) 100557. https://doi.org/10.1016/j.xcrp.2021.100557.
- 17. W. Liao, L. Qi, Y. Wang, J. Qin, G. Liu, S. Liang, H. He, L. Jiang, Interfacial engineering promoting electrosynthesis of ammonia over Mo/phosphotungstic acid with high performance, Adv. Funct. Mater. 31 (2021) 2009151. https://doi.org/10.1002/adfm.202009151.
- 18. W. Liao, K. Xie, L. Liu, X. Wang, Y. Luo, S. Liang, F. Liu, L. Jiang, Triggering in-plane defect cluster on MoS₂ for accelerated dinitrogen electroreduction to ammonia, J. Energy Chem. 62 (2021) 359-366. https://doi.org/10.1016/j.jechem.2021.03.043.
- 19. J.-D. Wang, Y.-H. Xie, Z.-F. Zhang, R.-Q. Liu, Z.-J. Li, Protonic conduction in Ca^{2+} -doped $La_2M_2O_7$ (M=Ce, Zr) with its application to ammonia synthesis electrochemically, Mater. Res. Bull. 40 (2005) 1294-1302. https://doi.org/10.1016/j.materresbull.2005.04.008.
- 20. R.-Q. Liu, Y.-H. Xie, J.-D. Wang, Z.-J. Li, B.-H. Wang, Synthesis of ammonia at atmospheric pressure with $Ce_{0.8}M_{0.2}O_{2-\delta}$ (M=La, Y, Gd, Sm) and their proton conduction at intermediate temperature, Solid State Ion. 177 (2006) 73-76. https://doi.org/10.1016/j.ssi.2005.07.018.
- 21. R. Lan, K. A. Alkhazmi, I. A. Amar, S. Tao, Synthesis of ammonia directly from wet air at intermediate temperature, Appl. Catal. B: Environ. 152-153 (2014) 212-217. https://doi.org/10.1016/j.apcatb.2014.01.037.
- 22. X. Zhu, *et al.* FeOOH quantum dots decorated graphene sheet: An efficient electrocatalyst for ambient N₂ reduction, Nano Res. 13 (2020) 209-214. https://doi.org/10.1007/s12274-019-2600-8.
- 23. Y. Wang, X. Zheng, D. Wang, Design concept for electrocatalysts, Nano Res. 15 (2022) 1730-1752. https://doi.org/10.1007/s12274-021-3794-0.
- 24. Y. Dong, I.-W. Chen, J. Li, Transverse and longitudinal degradations in ceramic solid electrolytes, Chem. Mater. in press, https://doi.org/10.1021/acs.chemmater.2c00329.
- 25. W. Bian, W. Wu, B. Wang, W. Tang, M. Zhou, C. Jin, H. Ding, W. Fan, Y. Dong, J. Li, D. Ding, Revitalizing interface in protonic ceramic cells by acid etch, Nature 604 (2022) 479. https://doi.org/10.1038/s41586-022-04457-y.
- 26. C. Duan, J. Huang, N. Sullivan, R. O'Hayre, Proton-conducting oxides for energy conversion and storage, Appl. Phys. Rev. 7 (2020) 011314. https://doi.org/10.1063/1.5135319.
- 27. L. Yang, S. Wang, K. Blinn, M. Liu, Z. Cheng, M. Liu, Enhanced sulfur and coking tolerance of a mixed ion conductor for SOFCs: BaZr_{0.1}Ce_{0.7}Y_{0.2-x}Yb_xO_{3-δ}, Science 326 (2009) 126-129. https://doi.org/10.1126/science.1174811.
- 28. S.H. Morejudo, R. Zanón, S. Escolástico, I. Yuste-Tirados, H. Malerød-Fjeld, P.

- K. Vestre, W. G. Coors, A. Martínez, T. Norby, J. M. Serra, C. Kjølseth, Direct conversion of methane to aromatics in a catalytic co-ionic membrane reactor, Science 353 (2016) 563-566. https://doi.org/10.1126/science.aag0274.
- 29. C. Duan, R. Kee, H. Zhu, N. Sullivan, L. Zhu, L. Bian, D. Jennings, R. O'Hayre, Highly efficient reversible protonic ceramic electrochemical cells for power generation and fuel production, Nat. Energy 4 (2019) 230-240. https://doi.org/10.1038/s41560-019-0333-2.
- 30. B. Hua, N. Yang, M. Li, Y.-Q. Zhang, Y.-F. Sun, J. Li, T. Etsell, P. Sarkar, K. Chuang, J.-L. Luo, Novel layered solid oxide fuel cells with multiple-twinned Ni_{0.8}Co_{0.2} nanoparticles: the key to thermally independent CO₂ utilization and power-chemical cogeneration, Energy Environ. Sci. 9 (2016) 207-215. https://doi.org/10.1039/C5EE03017J.
- 31. B. Hua, N. Yang, M. Li, Y.-F. Sun, Y.-Q. Zhang, J. Li, T. Etsell, P. Sarkar, J.-L. Luo, Anode-engineered protonic ceramic fuel cell with excellent performance and fuel compatibility, Adv. Mater. 28 (2016) 8922-8926. https://doi.org/10.1002/adma.201602103.
- 32. D. Ding, Y. Zhang, W. Wu, D. Chen, M. Liu, T. He, A novel low-thermal-budget approach for the co-production of ethylene and hydrogen via the electrochemical non-oxidative deprotonation of ethane, Energy Environ. Sci. 11 (2018) 1710-1716. https://doi.org/10.1039/C8EE00645H.
- 33. L. Lei, J. Zhang, Z. Yuan, J. Liu, M. Ni, F. Chen, Progress report on proton conducting solid oxide electrolysis cells, Adv. Funct. Mater. 29 (2019) 1903805. https://doi.org/10.1002/adfm.201903805.
- 34. J. Kästner, P. E. Blöchl, Ammonia production at the FeMo cofactor of nitrogenase: results from density functional theory, J. Am. Chem. Soc. 129 (2007) 2998-3006. https://doi.org/10.1021/ja068618h.
- 35. Q. J. Bruch, G. P. Connor, N. D. McMillion, A. S. Goldman, F. Hasanayan, P. L. Holland, A. J. M. Miller, Considering electrocatalytic ammonia synthesis via bimetallic dinitrogen cleavage, ACS Catal. 10 (2020) 10826-10846. https://doi.org/10.1021/acscatal.0c02606.
- 36. J. Zhang, X. Tian, M. Liu, H. Guo, J. Zhou, Q. Fang, Z. Liu, Q. Wu, J. Lou, Cobalt-modulated molybdenum–dinitrogen interaction in MoS₂ for catalyzing ammonia synthesis, J. Am. Chem. Soc. 141 (2019) 19269-19275. https://doi.org/10.1021/jacs.9b02501.
- 37. C. J. H. Jacobsen, S. Dahl, B. S. Clausen, S. Bahn, A. Logadottir, J. K. Nørskov, Catalyst design by interpolation in the periodic table: bimetallic ammonia synthesis catalysts, J. Am. Chem. Soc. 123 (2001) 8404-8405. https://doi.org/10.1021/ja010963d.
- 38. J. Li, *et al.* Constraining CO coverage on copper promotes high-efficiency ethylene electroproduction, Nat. Catal. 2 (2019) 1124-1131. https://doi.org/10.1038/s41929-019-0380-x.
- 39. M. M. Dubinin, The potential theory of adsorption of gases and vapors for adsorbents with energetically nonuniform surfaces, Chem. Rev. 60 (1960) 235-241.
- 40. H. Duan, *et al.* Molecular nitrogen promotes catalytic hydrodeoxygenation, Nat. Catal. 2 (2019) 1078-1087. https://doi.org/10.1038/s41929-019-0368-6.
- 41. J. K. Nørskov, Electronic factors in catalysis, Prog. Surf. Sci. 38 (1991) 103-144.
- 42. N. Saadatjou, A. Jafari, S. Sahebdelfar, Ruthenium nanocatalysts for ammonia synthesis: A review, Chem. Eng. Commun. 202 (2015) 420-448. https://doi.org/10.1080/00986445.2014.923995.

- 43. S. Back, Y. Jung, On the mechanism of electrochemical ammonia synthesis on the Ru catalyst, Phys. Chem. Chem. Phys. 18 (2016) 9161-9166. https://doi.org/10.1039/C5CP07363D.
- 44. H. Fang, D. Liu, Y. Luo, Y. Zhou, S. Liang, X. Wang, B. Lin, L. Jiang, Challenges and opportunities of Ru-based catalysts toward the synthesis and utilization of ammonia, ACS Catal. 12 (2022) 3938-3954. https://doi.org/10.1021/acscatal.2c00090.
- 45. M. T. Greiner, T. E. Jones, S. Beeg, L. Zwiener, M. Scherzer, F. Firgsdies, S. Piccinin, M. Armbrüster, A. Knop-Gericke, R. Schilögl, Free-atom-like d states in single-atom alloy catalysts, Nat. Chem. 10 (2018) 1008-1015. https://doi.org/10.1038/s41557-018-0125-5.
- 46. Y. Lum, *et al.* Tuning OH binding energy enables selective electrochemical oxidation of ethylene to ethylene glycol, Nat. Catal. 3 (2020) 14-22. https://doi.org/10.1038/s41929-019-0386-4.
- 47. E. Skúlason, T. Bligaard, S. Gudmundsdóttir, F. Studt, J. Rossmeisl, F. Abild-Pedersen, T. Vegge, H. Jónsson, J. K. Nørskov, A theoretical evaluation of possible transition metal electro-catalysts for N₂ reduction, Phys. Chem. Chem. Phys. 14 (2012) 1235-1245. https://doi.org/10.1039/C1CP22271F.
- 48. Y. Ogura, K. Sato, S.-i. Miyahara, Y. Kawano, T. Toriyama, T. Yamanoto, S. Matsumura, S. Hosokawa, K. Nagaoka, Efficient ammonia synthesis over a Ru/La_{0.5}Ce_{0.5}O_{1.75} catalyst pre-reduced at high temperature, Chem. Sci. 9 (2018) 2230-2237. https://doi.org/10.1039/C7SC05343F.
- 49. M. Li, B. Hua, J. Chen, Y. Zhong, J.-L. Luo, Charge transfer dynamics in RuO₂/perovskite nanohybrid for enhanced electrocatalysis in solid oxide electrolyzers, Nano Energy 57 (2019) 186-194. https://doi.org/10.1016/j.nanoen.2018.12.048.
- 50. M. Li, B. Hua, L.-C. Wang, J. D. Sugar, W. Wu, Y. Ding, J. Li, D. Ding, Switching of metal—oxygen hybridization for selective CO₂ electrohydrogenation under mild temperature and pressure, Nat. Catal. 4 (2021) 274-283. https://doi.org/10.1038/s41929-021-00590-5.
- 51. S. Xu, S. Chansai, S. Xu, C. E. Stere, Y. Jiao, S. Yang, C. Hardacre, X. Fan, CO poisoning of Ru catalysts in CO₂ hydrogenation under thermal and plasma conditions: a combined kinetic and diffuse reflectance infrared Fourier transform spectroscopy—mass spectrometry study, ACS Catal. 10 (2020) 12828-12840. https://dx.doi.org/10.1021/acscatal.0c03620.
- 52. D. Chandra, Y. Inoue, M. Sasase, M. Kitano, A. Bhaumik, K. Kamata, H. Hosono, M. Hara, A high performance catalyst of shape-specific ruthenium nanoparticles for production of primary amines by reductive amination of carbonyl compounds, Chem. Sci. 9 (2018) 5949-5956. https://doi.org/10.1039/C8SC01197D.
- 53. S. Xu, S. Chansai, Y. Shao, S. Xu, Y.-c. Wang, S. Haigh, Y. Mu, Y. Jiao, C. E. Stere, H. Chen, X. Fan, C. Hardacre, Mechanistic study of non-thermal plasma assisted CO₂ hydrogenation over Ru supported on MgAl layered double hydroxide, Appl. Catal. B: Environ. 268 (2020) 118752. https://doi.org/10.1016/j.apcatb.2020.118752.
- 54. X.-C. Hu, W.-W. Wang, R. Si, C. Ma, C.-J. Jia, Hydrogen production via catalytic decomposition of NH₃ using promoted MgO-supported ruthenium catalysts, Sci. China Chem. 62 (2019) 1625-1633. https://doi.org/10.1007/s11426-019-9578-8.
- 55. W. Zou, C. Ge, M. Lu, S. Wu, Y. Wang, J. Sun, Y. Pu, C. Tang, F. Gao, L. Dong, Engineering the NiO/CeO₂ interface to enhance the catalytic performance for CO oxidation, RSC Adv. 5 (2015) 98335-98343. https://doi.org/10.1039/C5RA20466F.
- 56. D. Goma, J. J. Delgado, L. Lefferts, J. Faria, J. J. Calvino, M. Á. Cauqui, Catalytic

- performance of Ni/CeO₂/X-ZrO₂ (X = Ca, Y) catalysts in the aqueous-phase reforming of methanol, Nanomater. 9 (2019) 1582. https://doi.org/doi:10.3390/nano9111582.
- 57. B. Hua, M. Li, Y.-F. Sun, Y.-Q. Zhang, N. Yan, J. Chen, T. Thundat, J. Li, J.-L. Luo, A coupling for success: Controlled growth of Co/CoO_x nanoshoots on perovskite mesoporous nanofibres as high-performance trifunctional electrocatalysts in alkaline condition, Nano Energy 32 (2017) 247-254. https://doi.org/10.1016/j.nanoen.2016.12.044.
- 58. H. Idriss, On the wrong assignment of the XPS O1s signal at 531–532 eV attributed to oxygen vacancies in photo- and electro-catalysts for water splitting and other materials applications, Surf. Sci. 712 (2021) 1221894. https://doi.org/10.1016/j.susc.2021.121894.
- 59. Schilling, C., Hofmann, A., Hess, C. & Ganduglia-Pirovano, M.V. Raman spectra of polycrystalline CeO₂: A density functional theory study, J. Phys. Chem. C 121 (2017) 20834-20849. https://doi.org/10.1021/acs.jpcc.7b06643.